Controlling four-wave mixing and six-wave mixing in a multi-Zeeman-sublevel atomic system with electromagnetically induced transparency

Yigang Du,[1] Yanpeng Zhang,[1,*] Cuicui Zuo,[1] Changbiao Li,[1] Zhiqiang Nie,[1] Huaibin Zheng,[1] Meizhen Shi,[1] Ruimin Wang,[1] Jianping Song,[1] Keqing Lu,[3] and Min Xiao[2,†]

[1]*Key Laboratory for Physical Electronics and Devices of the Ministry of Education and Shaanxi Key Laboratory of Information Photonic Technique, Xi'an Jiaotong University, Xi'an 710049, China*

[2]*Department of Physics, University of Arkansas, Fayetteville, Arkansas 72701, USA*

[3]*State Key Laboratory of Transient Optics and Technology, Xi'an Institute of Optics and Precision Mechanics, Chinese Academy of Sciences, Xi'an 710068, China*

(Received 3 February 2009; published 25 June 2009)

We theoretically investigate the dually dressed electromagnetically induced transparency, and the multidressed four-wave mixing (FWM) and six-wave mixing (SWM) processes in an inverted-*Y*-type atomic system with Zeeman sublevels. The results show that the Zeeman degeneracy of the dark states can be lifted by the dressing field as its intensity is increased. Moreover, the derived analytical expressions indicate that one can, for example, selectively create secondary dark states on the multi-Zeeman-sublevel dark states (by tuning the coupling field), distinguish two different types of dark states generated in two FWM processes (by properly controlling the coupling field intensity), and selectively enhance multi-FWM signals coming from various paths consisting of split Zeeman sublevels (by tuning the dressing field). The SWM signals can be either enhanced or suppressed by controlling the dressing field.

DOI: 10.1103/PhysRevA.79.063839 PACS number(s): 42.50.Gy, 42.65.Ky

I. INTRODUCTION

The effects of efficient high-order multiwave mixing processes have attracted a lot of interest in recent years [1–7]. Under the electromagnetically induced transparency (EIT) condition, not only the four-wave mixing (FWM) processes can be resonantly enhanced but also the generated FWM signals can be allowed to transmit through the atomic medium with little absorption [1–5,8–11]. Enhanced six-wave mixing (SWM) via induced atomic coherence was experimentally observed in a four-level inverted-*Y* (RY) atomic system [12,13]. Such SWM signal can be made to even coexist, compete, and spatially interfere with the FWM signal in the same system [14–16] by the assistance of EIT. Moreover, theoretical investigation on coexisting FWM, SWM, and EWM processes in a five-level system was also carried out [17]. The experimental demonstrations of these phenomena were often carried out in atomic systems, such as sodium and rubidium atomic vapors, in which each energy level actually consisted of several Zeeman sublevels interacting with different polarized light fields. However, for simplicity most theoretical analyses have been based on ideal level schemes which generally neglect Zeeman sublevels. Nevertheless, these analyses are reasonable in most cases because the differences will often be offset by the Doppler broadening when the sample is the hot atoms in a vapor cell. However, in certain cases, especially in the cold atomic samples, the effects of the multi-Zeeman-sublevels cannot be simply neglected.

For example, the investigations on the interactions of double EIT and the corresponding effects of atomic systems were done in recent years [18,19]. Effects due to dual-EIT windows with enhanced Kerr nonlinearity in a RY configuration considering no Zeeman sublevels were theoretically explored [20–22]. On the other hand, interesting effects with singly dressed EIT in a Λ-type three-level atomic system considering of multi-Zeeman-sublevels have been investigated both theoretically [23] and experimentally [24–26]. Furthermore, doubly dressed EIT in a tripod atomic system was demonstrated recently [27,28]. These works were carried out either in the cold atomic system or in vapor cells but with the atomic systems in the two-photon Doppler-free configuration [29]. In this work, we investigate the double-EIT dark states and their interactions in a realistic RY-type system with full consideration of the involved multi-Zeeman-sublevels. The stronger dressing field generates multi-Zeeman-sublevel dark states by inducing different spectral splits. The weaker coupling field can selectively create the secondarily dressed dark states on the generated multi-Zeeman-sublevel dark states by changing its frequency detuning.

Doubly dressed multiwave mixing and its three (i.e., nested, parallel, and sequential) dressed configurations have been theoretically investigated recently [17]. However, these previous works have only studied the ideal level systems without considering the multidressed multiwave mixing with multi-Zeeman-sublevels. Here, we focus our attention on understanding the FWM processes with multidressing fields in the RY system with multi-Zeeman-sublevel structures. Autler-Townes (AT) splitting spectrum shows several peak pairs which are from two different types of dark states generated in different transition processes. The enhanced transmission spectra clearly show a Zeeman characteristic feature which is induced by the multiple resonances due to the split Zeeman sublevels. We develop an analytical expression to determine the positions of the enhanced multiple peaks. The

*ypzhang@mail.xjtu.edu.cn
†mxiao@uark.edu

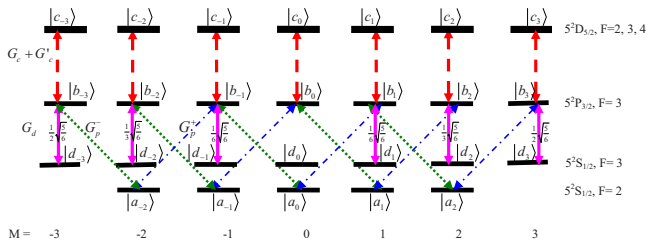

FIG. 1. (Color online) The RY-type system formed by linearly polarized probe, coupling fields, and dressing fields for ^{85}Rb atom. Solid, dotted, dashed-dotted, and dashed lines are transitions for linearly polarized dressing beams, left-circularly-polarized probe beam, right-circularly-polarized probe beam, and linearly polarized beam, respectively.

results confirm that we can selectively resonate the arbitrary transition paths of the FWM channels by tuning the frequency detuning of the dressing field. Finally, we will discuss the coexistence of the enhancement and suppression in the dually dressed SWM spectrum. Besides three enhanced peaks, one suppressed dip is also obtained simultaneously.

The paper is organized as follows. In Sec. II we derive the density-matrix equations of the RY system from the master equation. In Sec. III we present the simulations and results of this dual-EIT system with multi-Zeeman-sublevels. We discuss in Sec. IV, through simulations, the properties of the AT splitting, the suppression and enhancement of the triply dressed FWM signals. In Sec. V we show the coexistence of the suppression and enhancement of the SWM signals. Section VI gives a conclusion.

II. BASIC THEORY

This work refers to the real atomic system of ^{85}Rb as shown in Fig. 1. We denote states $5\ ^2S_{1/2}(F=2)$, $5\ ^2P_{3/2}(F=3)$, and $5\ ^2D_{5/2}$ ($F=2$, 3, and 4, since the frequency differences between these three hyperfine levels are less than 10 MHz, we consider them all together as degenerate), and $5\ ^2S_{1/2}(F=3)$ as $|a_M\rangle$, $|b_M\rangle$, $|c_M\rangle$, and $|d_M\rangle$, respectively. M indicates the magnetic quantum number. To emphasize the effects of the Zeeman sublevels, we consider a special setup for the polarized lasers beams similar to the one used in Ref. [26]. A linearly polarized probe field reduces to the two eigenstates of the polarization by a weak magnetic field which is in vertical direction. Namely, the right- and left-circularly polarized beams connect the transition from $|a_M\rangle$ to $|b_M\rangle$ with wave vectors $\mathbf{k}_p^{\pm}$, frequencies $\omega_p^{\pm}$, and Rabi frequencies $G_p^{\pm}$. Two linearly polarized coupling beams $G_c(\mathbf{k}_c,\omega_c)$ and $G_c'(\mathbf{k}_c',\omega_c)$ link $|b_M\rangle$ to $|c_M\rangle$, while one dressing beam $G_d(\mathbf{k}_d,\omega_d)$ drives the transition from $|b_M\rangle$ to $|d_M\rangle$, respectively. As shown in Fig. 1, this system consists of five right-circularly-polarized sub-RY systems (which are $|a_{-2}\rangle-|b_{-1}\rangle-|c_{-1}\rangle-|d_{-1}\rangle$, $|a_{-1}\rangle-|b_0\rangle-|c_0\rangle-|d_0\rangle$, $|a_0\rangle-|b_1\rangle-|c_1\rangle-|d_1\rangle$, $|a_1\rangle-|b_2\rangle-|c_2\rangle-|d_2\rangle$, and $|a_2\rangle-|b_3\rangle-|c_3\rangle-|d_3\rangle$, respectively) and five left-circularly-polarized sub-RY systems (which are $|a_{-2}\rangle-|b_{-3}\rangle-|c_{-3}\rangle-|d_{-3}\rangle$, $|a_{-1}\rangle-|b_{-2}\rangle-|c_{-2}\rangle-|d_{-2}\rangle$, $|a_0\rangle-|b_{-1}\rangle-|c_{-1}\rangle-|d_{-1}\rangle$, $|a_1\rangle-|b_0\rangle-|c_0\rangle-|d_0\rangle$, and $|a_2\rangle-|b_1\rangle-|c_1\rangle-|d_1\rangle$, respectively). Since transition from $|b_0\rangle$ to $|c_0\rangle$ is forbidden, $|a_{-1}\rangle-|b_0\rangle-|c_0\rangle-|d_0\rangle$ and $|a_1\rangle-|b_0\rangle-|c_0\rangle-|d_0\rangle$ are actually subladder systems. The probe beams with EIT generated FWM and SWM signals at frequency ω_p can coexist in this composite system [10–17].

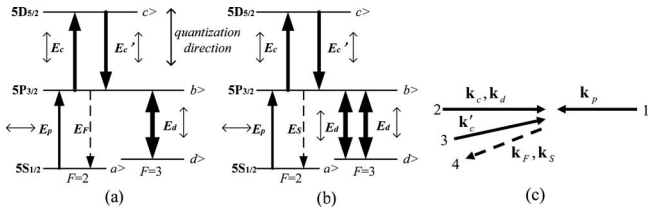

FIG. 2. [(a) and (b)] Energy diagrams for generating FWM and SWM signals. (c) Beam geometry used for the system.

Figure 2 shows the generation processes of the dressed FWM and SWM signals and their beam geometry. Figure 2(a) gives the FWM process generated by the probe beam E_p and two coupling beams (E_c and E_c') with the phase-matching condition of $\mathbf{k}_F=\mathbf{k}_p+\mathbf{k}_c-\mathbf{k}_c'$ via the perturbation channel of $\rho_{aa}^{(0)}\xrightarrow{\omega_p}\rho_{ba}^{(1)}\xrightarrow{\omega_c}\rho_{ca}^{(2)}\xrightarrow{-\omega_c}\rho_{ba}^{(3)}$ [10–17]. The probe polarization direction is orthogonal to the dressing and coupling fields' polarization, namely, the quantization axis direction. In fact, this FWM generation process can be viewed as a series of transitions: the first step is from $|a\rangle$ to $|b\rangle$ with absorption of a probe photon E_p, and the final state of this process can be dressed by the fields $E_d(G_d)$ and $E_c(G_c)$. The second step is the transition from $|b\rangle$ to $|c\rangle$ and the final state cannot be dressed by any field. The third step is the transition from $|c\rangle$ to $|b\rangle$ with the emission of a coupling photon E_c and the final state of this process can be dressed by $E_d(G_d)$. Then, the last transition is from $|b\rangle$ to $|a\rangle$, which emits a FWM photon at frequency ω_p. Thus, we can obtain the dressed perturbation chain: $\rho_{aa}^{(0)}\xrightarrow{\omega_p}\rho_{G_c\pm G_d\pm a}^{(1)}\xrightarrow{\omega_c}\rho_{ca}^{(2)}\xrightarrow{-\omega_c}\rho_{G_d\pm a}^{(3)}$. This comprehension and dressed perturbation chain will be helpful for deriving the FWM expression from the density-matrix equations below. Other than this FWM process, two possible SWM processes, via either the channel of $\rho_{aa}^{(0)}\xrightarrow{\omega_p}\rho_{ba}^{(1)}\xrightarrow{\omega_c}\rho_{ca}^{(2)}\xrightarrow{-\omega_c'}\rho_{ba}^{(3)}\xrightarrow{\omega_d}\rho_{da}^{(4)}\xrightarrow{-\omega_d}\rho_{ba}^{(5)}$ or $\rho_{aa}^{(0)}\xrightarrow{\omega_p}\rho_{ba}^{(1)}\xrightarrow{\omega_d}\rho_{da}^{(2)}\xrightarrow{-\omega_d}\rho_{ba}^{(3)}\xrightarrow{\omega_c}\rho_{ca}^{(4)}\xrightarrow{-\omega_c'}\rho_{ba}^{(5)}$, exist in this laser beam configuration, as shown in Fig. 2(b). Both of them use one photon from the probe beam E_p, two photons from the dressing beam E_d, and one photon each from E_c and E_c' with the same phase-matching condition of $\mathbf{k}_F=\mathbf{k}_p+\mathbf{k}_c-\mathbf{k}_c'+\mathbf{k}_d-\mathbf{k}_d$. These FWM and SWM processes can coexist and be phase matched to travel in the same direction as shown in Fig. 2(c).

The evolution of the atomic variables in the interaction representation is governed by the master equation

$$\frac{\partial\rho}{\partial t}=-\frac{i}{\hbar}[H_{\text{int}},\rho]+\left(\frac{\partial\rho}{\partial t}\right)_{inc}, \tag{1}$$

where the first term results from the coherent interaction and the second term represents dampings due to decay with or without emission, dephasing, and other irreversible processes. In the interaction representation and under the dipole

and rotating-wave approximation, the Hamiltonian for this system can be described as

$$H_{\text{int}} = -\hbar\Bigg[\sum_{M=-3}^{3}\Delta_p|b_M\rangle\langle b_M| + \sum_{M=-3}^{3}(\Delta_p+\Delta_c)|c_M\rangle\langle c_M| + \sum_{M=-3}^{3}(\Delta_p-\Delta_d)|d_M\rangle\langle d_M|\Bigg] - \hbar\Bigg(\sum_{M=-2}^{2}G_{pM}^{-}|a_M\rangle\langle b_{M-1}| + \sum_{M=-2}^{2}G_{pM}^{+}|a_M\rangle\langle b_{M+1}| + \text{c.c.}\Bigg) - \hbar\Bigg(\sum_{M=-3}^{3}G_{dM}|d_M\rangle\langle b_M| + \sum_{M=-3}^{3}G_{cM}|b_M\rangle\langle c_M| + \text{c.c.}\Bigg), \tag{2}$$

where $\Delta_p=\omega_{ab}-\omega_p$, $\Delta_c=\omega_{bc}-\omega_c$, and $\Delta_d=\omega_{db}-\omega_d$ are the frequency offsets of the probe, coupling, and dressing fields, respectively. $\omega_{ab},\omega_{bc},\omega_{db}$ are the transition frequencies from $|a\rangle$ to $|b\rangle$, $|b\rangle$ to $|c\rangle$, and $|d\rangle$ to $|b\rangle$, respectively. $G_{pM}^{+}=\mu_{aM,bM+1}E_p^{+}/\hbar$ and $G_{pM}^{-}=\mu_{aM,bM-1}E_p^{-}/\hbar$ $(M=-2,-1,\ldots,2)$, $G_{cM}=\mu_{bM,cM}E_c/\hbar$ and $G_{dM}=\mu_{bM,dM}E_d/\hbar$ $(M=-3,-2,\ldots,3)$ are the Rabi frequencies of the right-, left-circularly-polarized probe, coupling and dressing beams for various transitions between different Zeeman sublevels, respectively. $\mu_{iM,jM'}(i,j=a,b,c,d)$ are the transition dipole moments between various Zeeman sublevels, which can be calculated by the following expression [30]:

$$\mu_{iM,jM'} = \mu_{JJ}C_{ij}(M,M') = \mu_{JJ}(-1)^{2F'+J+I+M}\sqrt{(2F'+1)(2J+1)(2F+1)}\times\begin{Bmatrix} J & J' & 1\\ F' & F & I\end{Bmatrix}\begin{pmatrix} F' & 1 & F\\ M' & q & -M\end{pmatrix}, \tag{3}$$

where μ_{JJ} is the reduced dipole matrix element. $C_{ij}(M,M')$ are the Clebsch-Gordan (CG) coefficients. J,I,F are the quantum numbers of the total electron angular momentum, the total nuclear angular momentum, and the total atomic angular momentum, respectively. We define the standard Rabi frequencies as $G_p^{\pm}=\mu_{ab}E_p^{\pm}/\hbar$, $G_c=\mu_{bc}E_c/\hbar$, and $G_d=\mu_{bd}E_d/\hbar$, so the Rabi frequencies for the Zeeman sublevels can be easily expressed as $G_{pM}^{\pm}=C_{ab}(M,M\pm1)\times G_p^{\pm}$, $G_{cM}=C_{bc}(M,M)\times G_c$, and $G_{dM}=C_{bd}(M,M)\times G_d$, which indicate that the Rabi frequencies for various transitions among different Zeeman sublevels are generally different.

We consider the condition that the probe beams connecting different sub-RY systems are very weak, so these subsystems are basically independent of each other [27]. Under this condition, as to each subsystem, there are 16 density-matrix elements but only ten of them are independent. We write down few density-matrix equations from Eqs. (1) and (2), which are useful for the derivations below:

$$\frac{\partial\rho_{b_{M\pm1}a_M}}{\partial t} = -[i\Delta_p+\Gamma_{ba}]\rho_{b_{M\pm1}a_M} + iG_{p_M}^{\pm}\rho_{a_Ma_M} + iG_{c_{M\pm1}}^{*}\rho_{c_{M+1}a_M} + iG_{d_{M\pm1}}\rho_{d_{M\pm1}a_M} - iG_{p_M}^{\pm}\rho_{b_{M\pm1}b_{M\pm1}}, \tag{4a}$$

$$\frac{\partial\rho_{c_{M\pm1}a_M}}{\partial t} = -[i(\Delta_p+\Delta_c)+\Gamma_{ca}]\rho_{c_{M\pm1}a_M} + iG_{c_{M\pm1}}\rho_{b_{M\pm1}a_M} - iG_{p_M}^{\pm}\rho_{c_{M\pm1}b_{M\pm1}}, \tag{4b}$$

$$\frac{\partial\rho_{d_{M\pm1}a_M}}{\partial t} = -[i(\Delta_p-\Delta_d)+\Gamma_{da}]\rho_{d_{M\pm1}a_M} + iG_{d_{M\pm1}}^{*}\rho_{b_{M\pm1}a_M} - iG_{p_M}^{\pm}\rho_{d_{M\pm1}b_{M\pm1}} \quad (M=-2,-1,\ldots,2), \tag{4c}$$

where ρ_{ij} $(i,j=a,b,c,d)$ are the density-matrix elements. Γ_{ij} $(i,j=a,b,c,d)$ are the decay rates describing decays of populations and coherences mainly due to the spontaneous transitions. Decay rates between the same hyperfine levels but different Zeeman sublevels (i.e., $\Gamma_{iM,jM'}$) are generally different from each other. In this work, since the Rabi frequencies are always far greater than the decay rates, the difference in the decay rates between different Zeeman sublevels is neglected, which is now denoted as Γ_{ij} on the hyperfine levels to simplify our calculations. Otherwise, in the derivation below, the last term of each equation which contains the probe Rabi frequency will be neglected since the probe field is far weaker than the other two fields.

III. DUAL-DRESSED EIT

From the density-matrix equations (4), and under the weak probe fields and the steady-state approximations, we can obtain the expressions for the matrix elements of the probe beams:

$$\rho_{b_{M\pm1}a_M}^{\pm} = \frac{iG_{pM}^{\pm}}{i\Delta_p+\Gamma_{ba}+\dfrac{|G_{cM\pm1}|^2}{i(\Delta_p+\Delta_c)+\Gamma_{ca}}+\dfrac{|G_{dM\pm1}|^2}{i(\Delta_p-\Delta_d)+\Gamma_{da}}}\times\rho_{a_Ma_M}^{(0)} \quad (M=-2,-1,\ldots,2), \tag{5}$$

where $\rho_{a_Ma_M}^{(0)}$ is the population of the ground state $|a_M\rangle$. So the linear susceptibility containing the dressing effect of such ^{85}Rb atomic vapor can be written as

$$\chi = \sum_{M=-2}^{2}(\chi_{b_{M-1}a_M}^{-}+\chi_{b_{M+1}a_M}^{+}) = \frac{N}{\varepsilon_0\hbar}\Bigg[\sum_{M=-2}^{2}\Bigg(\frac{\mu_{b_{M+1}a_M}^2\rho_{b_{M+1}a_M}^{+}}{G_{pM}^{+}}+\frac{\mu_{b_{M-1}a_M}^2\rho_{b_{M-1}a_M}^{-}}{G_{pM}^{-}}\Bigg)\Bigg], \tag{6}$$

where N is the atom density. Then, the probe transmissivity T is given by

$$T=\exp[-2\pi L\,\text{Im}(\chi)/\lambda]. \tag{7}$$

Figure 3(a) depicts the calculated transmissivity of the probe beam versus the probe frequency detuning $\Delta_p/2\pi$ and the Rabi frequency of the dressing field $G_d/2\pi$. One can see that the EIT windows gradually emerge as increasing G_d. Figures 3(b)–3(f) show several cross sections of Fig. 3(a). When the dressing field is weak ($G_d=10$ MHz), as shown in

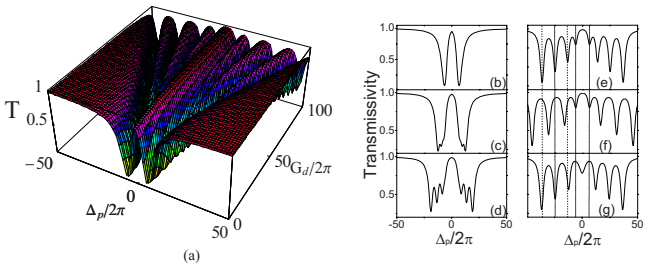

FIG. 3. (Color online) (a) Calculated transmissivity of the probe field versus $\Delta_p/2\pi$ and $G_d/2\pi$ when $G_c/2\pi=10$ MHz, $\Delta_c/2\pi=\Delta_d/2\pi=0$. [(b)–(f)] Several cross sections of (a) versus $\Delta_p/2\pi$ for $G_d/2\pi=10$, 25, 40, 80, and 100 MHz, respectively. (g) $G_d/2\pi=80$ MHz, $G_c/2\pi=0$, and $\Delta_c/2\pi=\Delta_d/2\pi=0$. The other parameters are $\Gamma_{ba}/2\pi=2.998$ MHz, $\Gamma_{ca}/2\pi=0.396$ MHz, $\Gamma_{da}/2\pi=0.1$ MHz, $\lambda=780.2$ nm, $N=1.5\times10^{11}/\mathrm{cm}^3$, and $\mu_{D2}=3.5843\times10^{-29}$ C m. The unit of the abscissa is MHz.

Fig. 3(b), only one EIT window appears, which indicates that all the splitting Zeeman sublevels are almost degenerate. However, as the dressing field intensity increases, more EIT windows appear and become clear in the spectrum, which probe the multi-dark-state structure of this system [24].

We can easily explain this phenomenon from Eq. (5). In the denominator, the dressing field G_d and the coupling field G_c are related in a summation, which is considered as in the sequentially dressed scheme [17]. In such case, the two fields are intermixed and cannot be divided at the resonant condition of $\Delta_c=\Delta_d=0$. They split one energy level into two dressed states giving only two absorption peaks in the spectrum. In the limit of $|G_{cM\pm1}|^2+|G_{dM\pm1}|^2\gg\Gamma_{ca}\Gamma_{da}$, positions of the split peaks (or equally, split levels) are at $\Delta_{pM}=\pm(|G_{cM\pm1}|^2+|G_{dM\pm1}|^2)^{1/2}$. Different CG coefficients give different Rabi frequencies, and therefore different splitting distances, so multiple absorption peaks emerge [24]. For the linearly polarized dressing field, CG coefficients are symmetric with respect to $M=0$, namely, $C_{ij}(M,M)=C_{ij}(-M,-M)$. Hence, the symmetrical Zeeman sublevels must always be degenerate. Furthermore, from the values of CG coefficients, we can conclude that the absorption peak pairs from inner to outer frequencies in the spectrum are caused by Zeeman sublevels $M=0$, $M=\pm1$, $M=\pm2$, and $M=\pm3$ respectively. These results are consistent with the ones obtained in Ref. [24] which used singly dressed EIT scheme in multi-Λ-type subsystems involving Zeeman sublevels. Note that the sublevel $M=0$ is split only by the weak coupling field ($G_c/2\pi=10$ MHz) because of $G_{d,M=0}=0$ (transition forbidden). Comparisons of Figs. 3(e)–3(g) can confirm this conclusion, i.e., as G_d [in Figs. 3(e) and 3(f)] increases, the inner peak pair does not move; however when the coupling field is blocked [Fig. 3(g) and comparing to Fig. 3(e)], the inner peaks fuse together.

Figure 3 shows the variations in the probe spectrum as the dressing field intensity is increased when it is on resonant and the dark states induced by the two fields are completely overlapped. Now, we tune the coupling field ($\Delta_c/2\pi=0$, 17, 33, and 45 MHz) under the same conditions as in Fig. 3(f). As Fig. 4(a) shows, the coupling field splits each absorption peak generated by the dressing field. The peaks (probing the

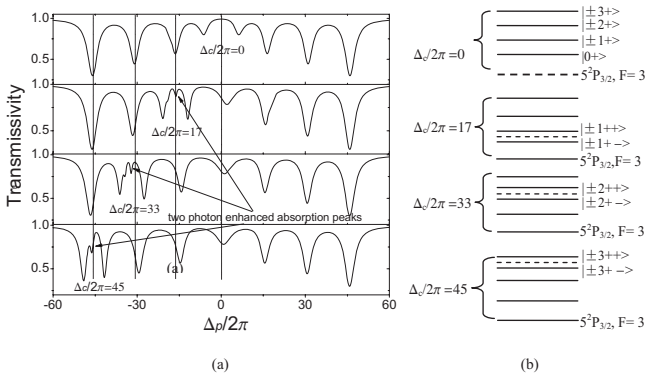

FIG. 4. (a) Calculated transmissivity of the probe beam versus $\Delta_p/2\pi$ for $\Delta_c/2\pi=0,17,33,45$ MHz, respectively, when $G_d/2\pi=100$ MHz, $G_c/2\pi=10$ MHz, and $\Delta_d/2\pi=0$. (b) Diagram of positive levels (including secondary splitting) of $5\ ^2P_{3/2}$, $F=3$ corresponding to (a). Other parameters are the same as in Fig. 3. The unit of the abscissa is MHz.

shifted Zeeman sublevels) are split again by the coupling field, as shown in Fig. 4(b) (only the positive split levels are shown). The small peak in each secondary EIT window is the two-photon-enhanced absorption peaks, which is generated by the two-photon (the detuned coupling and probe fields which hit the same position) resonance-enhanced absorption with the other split Zeeman sublevels which are not secondarily split by the coupling field.

Therefore, under resonant condition, the dark states with multi-Zeeman-sublevels are lifted by the strong dressing field because of the differences in the CG coefficients. The coupling and dressing fields are intermixed and enhanced with each other. When it is frequency detuned, the coupling field can selectively create secondary dark states on the split levels generated by the dressing field.

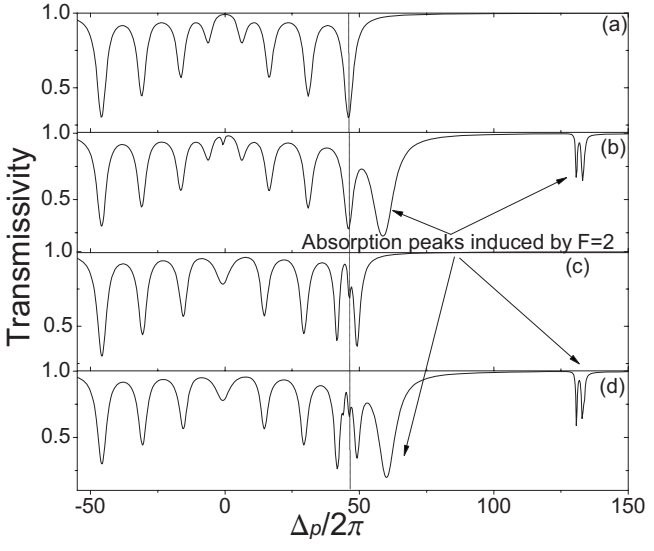

FIG. 5. [(a) and (b)] Comparison of the cases of whether to consider the hyperfine level $F=2$ or not at the same condition of Fig. 3(f). [(c) and (d)] Comparison of the cases of whether to consider the hyperfine level $F=2$ or not at the similar condition (with just an opposite detuning of $\Delta_c/2\pi=-45$ MHz) of the fourth figure of Fig. 4(a). The unit of the abscissa is MHz.

The discussions above are all under the condition of not considering the other hyperfine levels. However, for the real ^{85}Rb atomic systems in experiments related to narrow spectra, the multihyperfine levels should be considered. Figure 5 gives the comparison of the probe transmissivity with and without the hyperfine level $F=2$, which is the nearest hyperfine level of $F=3$ (63.4 MHz below $F=3$). Figures 5(a) and 5(b) are the comparison corresponding to Fig. 3(f) while Figs. 5(c) and 5(d) are the comparison at the similar condition as the fourth figure of Fig. 4(a) (with just an opposite detuning of $\Delta_c/2\pi=-45$ MHz). We can see that the peaks induced by the hyperfine level $F=2$ do not mix with $F=3$ when proper dressing beam intensity and frequency offset are used. So, if one wishes to distinguish peaks from different hyperfine levels or to avoid the contributions from other hyperfine levels, the frequency offset and detuning of the laser beams have to be carefully controlled.

Fully simulating the spectra with all hyperfine levels can be done by simply summing over all the hyperfine levels' contributions for the permitting transitions. However, since such spectra will be too complicated to see the physics behind, we will avoid the contribution from other hyperfine levels and minimize their impacts.

IV. FOUR-WAVE MIXING

By using the dressed perturbation chain $\rho_{aa}^{(0)} \overset{\omega_p}{\rightarrow} \rho_{G_c \pm G_d \pm a}^{(1)} \overset{\omega_c}{\rightarrow} \rho_{ca}^{(2)} \overset{-\omega_c}{\rightarrow} \rho_{G_d \pm a}^{(3)}$, we can obtain the expressions for FWM from the density-matrix equations under similar approximations as for EIT:

$$\rho_{b_{M\pm1}a_M}^{(3)\pm} = -\frac{iG_{pM}^{\pm}|G_{cM\pm1}|^2}{i\Delta_p+\Gamma_{ba}+\dfrac{|G_{cM\pm1}|^2}{i(\Delta_p+\Delta_c)+\Gamma_{ca}}+\dfrac{|G_{dM\pm1}|^2}{i(\Delta_p-\Delta_d)+\Gamma_{da}}} \frac{1}{i\Delta_p+\Gamma_{ba}+\dfrac{|G_{dM\pm1}|^2}{i(\Delta_p-\Delta_d)+\Gamma_{da}}} \frac{1}{i(\Delta_p+\Delta_c)+\Gamma_{ca}}$$
$$(M=-2,-1,\ldots,2). \tag{8}$$

The signal intensity I is proportional to $|N\mu_1\rho|^2$, so the relative FWM signal intensity is given by

$$I_F \propto \left| \sum_{M=-2}^{2} (\mu_{b_{M+1}a_M}\rho_{b_{M+1}a_M}^{(3)+} + \mu_{b_{M-1}a_M}\rho_{b_{M-1}a_M}^{(3)-}) \right|^2. \tag{9}$$

In order to clearly understand the simulation results, let us analyze the complex expressions as given by Eq. (8). For each expression, there are three production terms. In the denominator of the first term, the Rabi frequencies of the two fields ($G_{cM\pm1}$ and $G_{dM\pm1}$) are in sequential-dressing scheme like the expressions for EIT. $G_{dM\pm1}$ in the denominator of the second term multiply the sequential term, which can be denoted as a parallel-dressing scheme [17]. Therefore, the expression of FWM is a combination of a sequentially dressed scheme and a singly dressed scheme. As to the parallel scheme, which is different from the entanglement of two sequential fields, its two multiplying parts do not necessarily interact with each other. So, the two parallel terms may give two independent groups of peaks. Peaks in one group induced by the sequentially dressed term are located at $\Delta_{pM}=\pm(|G_{cM\pm1}|^2+|G_{dM\pm1}|^2)^{1/2}$, and the peaks from the other group induced by the singly dressed term are at $\Delta_{pM}=\pm G_{dM\pm1}$.

Figure 6 is the calculated relative intensity of FWM signal for different Rabi frequencies of the dressing and coupling fields. Seven irregular peak pairs (which are denoted as $1,2,\ldots,7$ from lower to higher offset, respectively) are obtained (the single peak in the center is generated by the two-photon term of the expression which is not our focus of discussion here). However, from comparing the three curves in Fig. 6, we can well understand the complex peak structures. For curves (a) and (b), as G_c is changed but not G_d, peaks (pairs) 2, 3, 5, and 7 shift, while peaks 1, 4, and 6 are stable. So, peaks 2, 3, 5, and 7 are generated by the sequential-dressing term (G_c and G_d) which probes the group of multi-Zeeman-sublevel dark states generated in the first transition of the FWM process. Peaks 1, 4 and 6, however, are split by the singly dressed parallel G_d, which probes the other group of dark states generated in the third transition of

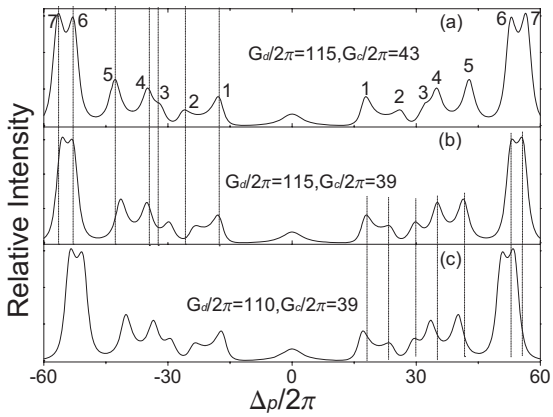

FIG. 6. Intensity of the FWM signal versus $\Delta_p/2\pi$ for (a) $G_c/2\pi=43$ MHz, $G_d/2\pi=115$ MHz; (b) $G_c/2\pi=39$ MHz, $G_d/2\pi=115$ MHz; (c) $G_c/2\pi=39$ MHz, $G_d/2\pi=110$ MHz. The parameters are $\Delta_c/2\pi=\Delta_d/2\pi=0$, $G_p/2\pi=2$ MHz, and the others are the same as in Fig. 3. The unit of the abscissa is MHz.

the FWM process. For curves (b) and (c), as G_d is changed but not G_c, peak 2 is stable while the other peaks move. Similar to EIT, peak 2 must be split only by G_c, since $G_d=0$ for Zeeman sublevel $M=0$. Looking at the values of CG coefficients, we can decide which peaks of the two groups are induced by which Zeeman sublevels. By using the expressions of the peak positions, we can calculate the positions of the peaks for curve (b) as $\Delta_{peak1}=\pm G_{d,\pm1}/2\pi=\pm 17.5$ MHz, $\Delta_{peak2}=\pm G_{c,0}/2\pi=\pm 24.3$ MHz, $\Delta_{peak3}=\pm(|G_{c,\pm1}|^2+|G_{d,\pm1}|^2)^{1/2}/2\pi=\pm 29.6$ MHz, $\Delta_{peak4}=\pm|G_{d,\pm2}|/2\pi=\pm 35$ MHz, $\Delta_{peak5}=\pm(|G_{c,\pm2}|^2+|G_{d,\pm2}|^2)^{1/2}/2\pi=\pm 41.6$ MHz, $\Delta_{peak6}=\pm G_{d,\pm3}/2\pi=\pm 52.5$ MHz, and $\Delta_{peak7}=\pm(|G_{c,\pm3}|^2+|G_{d,\pm3}|^2)^{1/2}/2\pi=\pm 56.2$ MHz. The numerically calculated maxima in curve (b) are at ± 17.9496, ± 23.2243, ± 29.837, ± 35.1064, ± 41.3738, ± 53.2318, and ± 55.4742 MHz, respectively, which agree very well with the analytically calculated results, confirming that the expressions are reasonable. Properly intensity of the dressing and coupling fields were controlled for avoiding bringing hyperfine levels $F=2$ and $F=1$ in our discussion.

As discussed above, the sequentially dressed scheme induces one group of multi-Zeeman-sublevel dark states and the parallel singly dressed field induces the other group which does not interact with the first group. The basic reason for such phenomenon is that the parallel dressing scheme represents two transition processes in FWM. The two groups of multi-Zeeman-sublevel dark states generated in different processes are distinguishable because the weaker coupling field enhances the dressed effect of the dressing field in the first transition process.

For better understanding the enhancement and suppression effects of the signals, we divide Eq. (8) by the original FWM expression which has no dressing fields [i.e., let G_c and G_d in the denominator of Eq. (8) equal to 0]. In such case, when the signal intensity is below one, it means suppression of FWM, while above one means enhancement of FWM signal intensity. The expression for normalized FWM signal with dressing fields reduces to

$$\tilde{\rho}^{(3)\pm}_{b_{M\pm1}a_M}=\frac{(i\Delta_p+\Gamma_{ba})^2}{i\Delta_p+\Gamma_{ba}+\dfrac{|G_{cM\pm1}|^2}{i(\Delta_p+\Delta_c)+\Gamma_{ca}}+\dfrac{|G_{dM\pm1}|^2}{i(\Delta_p-\Delta_d)+\Gamma_{da}}}\frac{1}{i\Delta_p+\Gamma_{ba}+\dfrac{|G_{dM\pm1}|^2}{i(\Delta_p-\Delta_d)+\Gamma_{da}}}\quad(M=-2,-1,\ldots,2). \tag{10}$$

The normalized FWM signal intensity is given by

$$\tilde{I}_F\propto\left|\sum_{M=-2}^{2}(\mu_{b_{M+1}a_M}\tilde{\rho}^{(3)+}_{b_{M+1}a_M}+\mu_{b_{M-1}a_M}\tilde{\rho}^{(3)-}_{b_{M-1}a_M})\right|^2. \tag{11}$$

Figure 7(a) depicts the intensity of the dressed FWM signal as $\Delta_c/2\pi$ and $\Delta_d/2\pi$ are scanned with $\Delta_p/2\pi=-60$ MHz. [To avoid the hyperfine level $F=2$, we choose $\Delta_p/2\pi<0$ since for the probe field, the hyperfine level $F=4$ over $F=3$ is forbidden transition level (transition $5S_{1/2}$, $F=2\rightarrow 5P_{3/2}$, $F=4$ is forbidden), so it cannot involve other hyperfine levels other than the $F=3$ while the intensity is not strong enough.] The field strengths are $G_d/2\pi=100$ MHz, $G_c/2\pi=15$ MHz, and $G_p/2\pi=3$ MHz and the other parameters are the same as in Fig. 3. A cross section of Fig. 7(a) versus $\Delta_d/2\pi$ (when $\Delta_c/2\pi=0$), as shown in Fig. 7(b), shows three enhanced peaks, which is different from the case with only one enhanced peak in each curve in Ref. [17]. Surely, the multi-Zeeman splitting sublevels induced by the dressing fields are responsible for this phenomenon. As for the first transition process, the enhancement condition is $\Delta_p-\Delta_{pM}=0$, where Δ_{pM} is the frequency shift of the given Zeeman sublevel (M). This represents the new resonant condition between the probe field and the splitting levels in the dressed-state picture. As shown in Fig. 7(c) (the coupling beam is omitted because of its less contribution in this case), the probe detuning is fixed at $\Delta_p/2\pi=-60$ MHz, the split Zeeman sublevels move as the dressing field is scanned. Only three positive splitting levels can get through the resonant position ($\Delta_p/2\pi=-60$ MHz). If any of them are set at this position [dashed line in Fig. 7(c)], it will satisfy the enhancement condition and greatly enhance the FWM signal. So the three negative splitting levels generate three enhanced FWM peaks when the dressing field is scanned [as shown in Fig. 7(c) (I-III)]. The huge values in the y axis are caused by the parallel-dressing scheme since the two simultaneously enhanced terms are multiplied.

Now let us derive the analytical expressions for the enhancement positions. By using Eq. (10) and under the approximations of G_d, Δ_d, and $\Delta_p\gg G_c>\Gamma_{ba}$, we can obtain the locations of the splitting levels relative to the original position of the state $|b\rangle$ as

$$\Delta_{pM}=\frac{1}{2}(\Delta_d\pm\sqrt{\Delta_d^2+4|G_{dM}|^2}). \tag{12}$$

Combining this with the enhancement condition of $\Delta_p-\Delta_{pM}=0$, the detuning values for the dressing field, when the FWM is enhanced, can be determined to be

$$\Delta_{dM}=(\Delta_p^2-|G_{dM}|^2)/\Delta_p. \tag{13}$$

According to Fig. 7(b), the three enhanced peaks are located at $\Delta_d/2\pi=-25.278$, -44.568, and -56.142 MHz. The calculated positions for the three maxima are -24.968, -44.392, and -56.083 MHz, respectively, which show very good agreements.

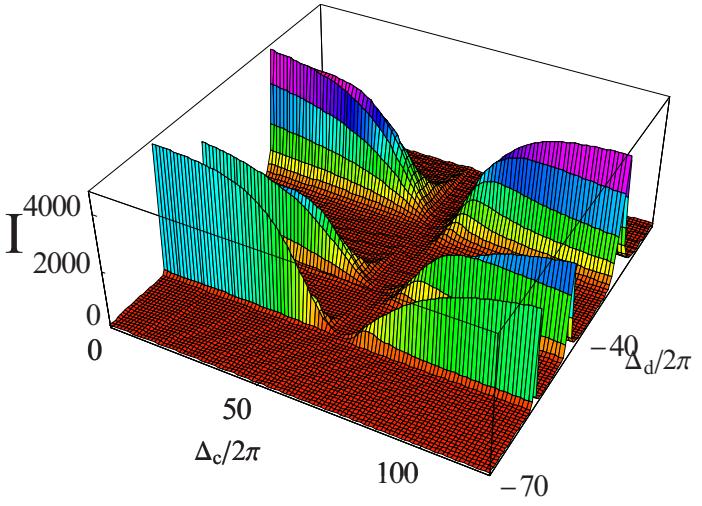

(a)

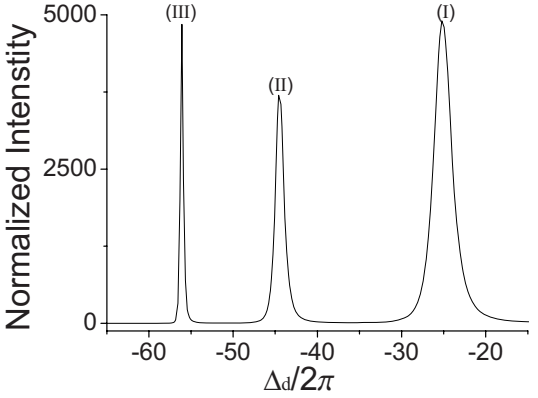

(b)

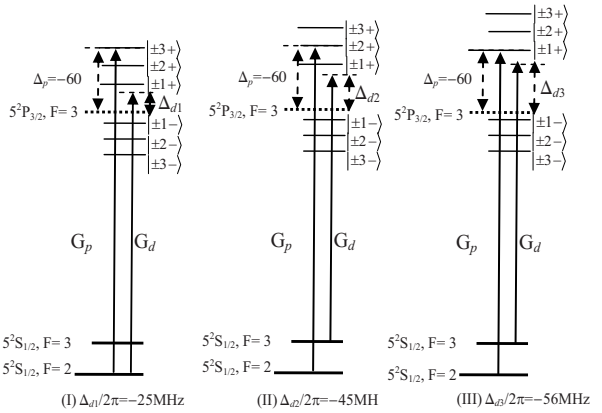

(c)

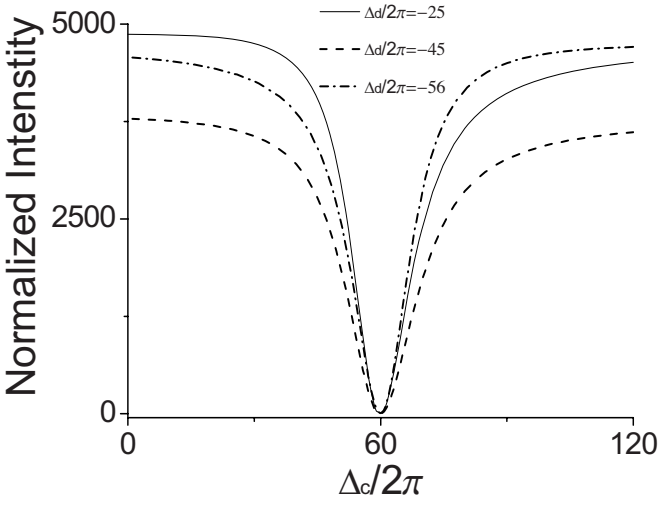

(d)

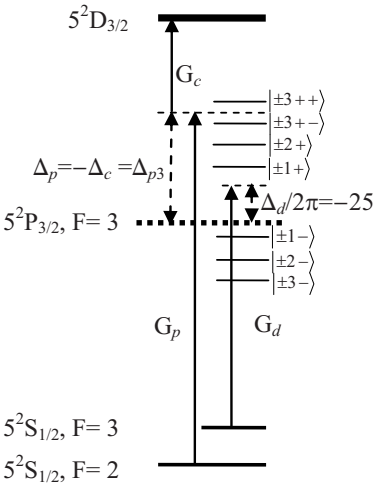

(e)

FIG. 7. (Color online) (a) Intensity of FWM signal versus $\Delta_c/2\pi$ and $\Delta_d/2\pi$ with $\Delta_p/2\pi=-60$ MHz. The parameters are $G_d/2\pi=100$ MHz, $G_c/2\pi=15$ MHz, and $G_p/2\pi=3$ MHz; the other parameters are the same as in Fig. 3(b). Cross section of (a) versus $\Delta_d/2\pi$ for $\Delta_c/2\pi=0$. (c) Schematic dressed-state diagram for the enhancement corresponding to (b). (d) Cross sections of (a) versus $\Delta_c/2\pi$ for $\Delta_d/2\pi=-25$ MHz (solid line), −45 MHz (dash-dotted line), and −56 MHz (dash-dotted line), respectively. (e) Schematic dressed-state diagram for the suppression of FWM signal corresponding to (d) (the solid line with $\Delta_d/2\pi=-25$ MHz). The unit of the abscissa is MHz.

Figure 7(d) presents several cross sections of Fig. 7(a) versus $\Delta_c/2\pi$ for $\Delta_d/2\pi=-25$, -45, and -56 MHz. These three curves all give the same dip at $\Delta_c/2\pi=60$ MHz on the enhancement background. This means that the coupling field greatly suppresses the FWM signals which have been enhanced by the dressing field [as shown in Fig. 7(b)]. In fact, this obeys the suppression condition $\Delta_p+\Delta_c=0$, at which the coupling and probe fields hit the same position in frequency. So the probability for the probe photon transition at $\Delta_p=-\Delta_c$ has been greatly reduced because of the dressing effect of the coupling field, even when the enhancement condition is also satisfied. Figure 7(e) shows the diagram for the split levels when $\Delta_c/2\pi=60$ MHz and $\Delta_d/2\pi=-25$ MHz. The split sublevels $|\pm 3+\rangle$ are further split into $|\pm 3++\rangle$ and $|\pm 3+-\rangle$, respectively, by the coupling field, similar to the secondary dressing in EIT case, so the FWM signal is suppressed.

Therefore, the spectrum of the FWM signal versus the dressing field detuning can also reveal the Zeeman structure in the atomic system. This is triple single-photon resonance ($\Delta_p=0$) enhancements of FWM processes in split Zeeman sublevels. The analytical expressions for the positions of the dressing field fixed show that we can selectively enhance each FWM path consisting of different split Zeeman sublevels. At the same time, secondary dressing effects, induced by the coupling field like in the EIT case, also exist in the FWM spectrum and can greatly suppress the FWM signal.

V. SIX-WAVE MIXING

Using similar derivation procedure as for FWM processes in the last section, by means of the density-matrix equations and two SWM perturbation chains and under similar approximation, we can obtain the expressions for dressed SWM processes as [17]

$$\rho^{(5)\pm}_{b_{M\pm1}a_M}=\frac{iG^{\pm}_{pM}|G_{cM\pm1}|^2|G_{dM\pm1}|^2}{i\Delta_p+\Gamma_{ba}+\dfrac{|G_{cM\pm1}|^2}{i(\Delta_p+\Delta_c)+\Gamma_{ca}}}\times\frac{1}{i\Delta_p+\Gamma_{ba}+\dfrac{|G_{dM\pm1}|^2}{i(\Delta_p-\Delta_d)+\Gamma_{da}}}\times\frac{1}{i(\Delta_p-\Delta_d)+\Gamma_{da}}\frac{1}{i\Delta_p+\Gamma_{ba}}\frac{1}{i(\Delta_p+\Delta_c)+\Gamma_{ca}}$$
$$(M=-2,-1,\ldots,2). \quad (14)$$

The normalized expressions for the dressed SWM signals (by dividing the original SWM expression without the dressing fields) with multi-Zeeman-sublevels are

$$\tilde{\rho}^{(5)\pm}_{b_{M\pm1}a_M}=\frac{(i\Delta_p+\Gamma_{ba})^2}{i\Delta_p+\Gamma_{ba}+\dfrac{|G_{cM\pm1}|^2}{i(\Delta_p+\Delta_c)+\Gamma_{ca}}}\times\frac{1}{i\Delta_p+\Gamma_{ba}+\dfrac{|G_{dM\pm1}|^2}{i(\Delta_p-\Delta_d)+\Gamma_{da}}},$$
$$(M=-2,-1,\ldots,2). \quad (15)$$

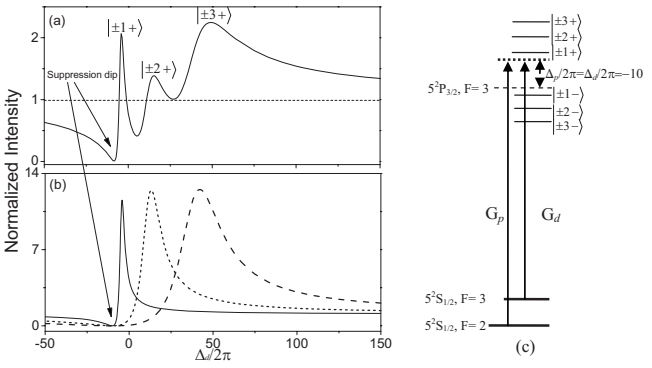

FIG. 8. (a) Intensity of SWM signal versus $\Delta_d/2\pi$ with $\Delta_p/2\pi=-10$ MHz. The parameters are $G_d/2\pi=50$ MHz, $G_c/2\pi=10$ MHz, and $G_p/2\pi=3$ MHz, $\Delta_c/2\pi=100$ MHz; the other parameters are the same as in Fig. 3(b). The curves show structures as singly induced by $|\pm 3+\rangle$ (dashed line), $|\pm 2+\rangle$ (dotted line), and $|\pm 1+\rangle$ (solid line), respectively, under the same condition as in (a). (c) Schematic dressed-state diagram for the signal enhancement corresponding to (a). The unit of the abscissa is MHz.

Since the signal intensity I is proportional to $|N\mu_1\rho|^2$, the relative SWM signal intensities (normalized) are given by

$$\tilde{I}_S=\left|\sum_{M=-2}^{2}(\mu_{b_{M+1}a_M}\tilde{\rho}^{(5)+}_{b_{M+1}a_M}+\mu_{b_{M-1}a_M}\tilde{\rho}^{(5)-}_{b_{M-1}a_M})\right|^2. \quad (16)$$

Since the basic analyses and major results of AT splitting in the SWM case are similar to the case of FWM, as discussed in the last section, we will not repeat the discussions here.

Figure 8(a) is the normalized SWM intensity according to Eq. (15) versus $\Delta_d/2\pi$ when the probe beam is slightly detuned ($\Delta_p/2\pi=-10$ MHz). Other parameters are $G_d/2\pi=50$ MHz, $G_c/2\pi=10$ MHz, and $\Delta_c/2\pi=100$ MHz. Similar to the FWM enhancement spectrum, three enhanced peaks (from left to right) are induced by the single-photon resonances of the probe beam with the dressed states $|\pm 3+\rangle$, $|\pm 2+\rangle$, and $|\pm 1+\rangle$, respectively. The curves of Fig. 8(b) are respective singly induced by $|\pm 3+\rangle$ (dashed line), $|\pm 2+\rangle$ (dotted line), and $|\pm 1+\rangle$ (solid line) under the same condition as in Fig. 8(a), which show different enhanced peaks (different positions).

Also, one suppression dip exists. Because of the suppression condition of $\Delta_p-\Delta_d=0$, only one suppression dip can exist at $\Delta_d/2\pi=\Delta_p/2\pi=-10$ MHz for all the split Zeeman sublevels. Figures 8(a) and 8(b) both confirm this conclusion. Figure 8(c) is the schematic dressed-state diagram to show the condition for suppression. One can see that as the dressing field hits the position of the probe field, it effectively suppresses its transition, and therefore reduces the SWM process.

Therefore, as the dressing field is scanned in frequency, the SWM signal gets not only multiple enhancement peaks, but also suppression dips when the probe field is slightly detuned. The mechanism for enhancement is similar to the one as in FWM. The suppressed dips, however, represent the dressed effects of the dressing field, which cannot reveal the Zeeman structure in the system.

VI. CONCLUSION

The effects of multidressing fields on the probe, FWM, and SWM signals in an atomic system with multi-Zeeman-sublevels are theoretically investigated in detail. As the dressing field intensities are increased, multi-Zeeman-sublevel dark state peaks appear in the transmission spectra, indicating different shifting frequencies of various Zeeman sublevels because of different CG coefficients. By using a weaker coupling field to selectively dress the AT peaks generated by the dressing field, secondarily dressed peaks in EIT are obtained. In AT splitting spectrum for FWM signal, two groups of peaks are shown to reflect different dark states generated in two transition processes of FWM by choosing right coupling field intensity. In the spectrum of the enhanced FWM signals, the Zeeman characteristics in the enhanced peaks reflect the multi-single-photon resonances of the probe beam with the split Zeeman sublevels. The SWM spectrum in this system with multi-Zeeman-sublevels shows not only enhanced peaks but also suppressed dips. Moreover, the analytically calculated positions of AT peaks and enhanced/suppressed peak positions using simple dark-state analyses are in good agreement with the numerically calculated maxima, confirming that the complicated multi-Zeeman-sublevel dark states can be well controlled by dressing fields. These dressed-state analyses and simulation results in the practical atomic system with Zeeman sublevels are very important in better understanding the AT splitting, enhancement, and suppression of multiwave mixing signals in real atomic systems for experimental investigations.

The simultaneous FWM and SWM processes can interfere since their signal photons are in the same transition. First, by making use of atomic coherence induced by the dressing fields, the SWM signal can be greatly enhanced and even made to be in the same order of magnitude as the coexisting FWM signal. Second, with a specially designed spatial configuration for phase matching, the directions of the FWM and SWM signals can be controlled, so if they are spatially overlapping, clear interference can be observed. Finally, an appropriate optical delay (introduced in the dressing beam E_d) can create a controllable phase difference between the FWM and SWM processes, and therefore control the interference. Such manipulations of high-order nonlinear optical processes and their interplays in multilevel atomic systems can have potential applications in coherent quantum control, nonlinear optical spectroscopy, precision measurements, and quantum information processing.

ACKNOWLEDGMENTS

This work was supported by NNSFC (Grant No. 60678005), FANEDD (Grant No. 200339), RFDP (Grant No. 20050698017), FYTEFYTIHEC (Grant No. 101061), and NCET (Grant No. 08-0431).

[1] P. R. Hemmer, D. P. Katz, J. Donoghue, M. Cronin-Golomb, M. S. Shahriar, and P. Kumar, Opt. Lett. **20**, 982 (1995).
[2] Y. Li and M. Xiao, Opt. Lett. **21**, 1064 (1996); B. Lu, W. H. Burkett, and M. Xiao, *ibid.* **23**, 804 (1998).
[3] M. M. Kash, V. A. Sautenkov, A. S. Zibrov, L. Hollberg, G. R. Welch, M. D. Lukin, Y. Rostovtsev, E. S. Fry, and M. O. Scully, Phys. Rev. Lett. **82**, 5229 (1999).
[4] D. A. Braje, V. Balic, S. Goda, G. Y. Yin, and S. E. Harris, Phys. Rev. Lett. **93**, 183601 (2004).
[5] H. Kang, G. Hernandez, and Y. F. Zhu, Phys. Rev. A **70**, 061804 (2004).
[6] H. Kang, G. Hernandez, and Y. F. Zhu, Phys. Rev. Lett. **93**, 073601 (2004).
[7] Z. C. Zuo, J. Sun, X. Liu, Q. Jiang, G. S. Fu, L. A. Wu, and P. M. Fu, Phys. Rev. Lett. **97**, 193904 (2006).
[8] S. E. Harris, Phys. Today **50** (7), 36 (1997).
[9] Y. Wu, J. Saldana, and Y. F. Zhu, Phys. Rev. A **67**, 013811 (2003); Y. Wu and L. Deng, Phys. Rev. Lett. **93**, 143904 (2004).
[10] Y. P. Zhang *et al.*, Opt. Lett. **32**, 1120 (2007).
[11] Y. P. Zhang, B. Anderson, and M. Xiao, Appl. Phys. Lett. **91**, 061113 (2007).
[12] Y. P. Zhang and M. Xiao, Appl. Phys. Lett. **90**, 111104 (2007).
[13] Y. P. Zhang *et al.*, Phys. Rev. A **77**, 061801(R) (2008).
[14] Y. P. Zhang, A. W. Brown, and M. Xiao, Phys. Rev. Lett. **99**, 123603 (2007).
[15] Y. P. Zhang, U. Khadka, B. Anderson, and M. Xiao, Phys. Rev. Lett. **102**, 013601 (2009).
[16] Y. P. Zhang, B. Anderson, A. W. Brown, and M. Xiao, Appl. Phys. Lett. **91**, 221108 (2007).
[17] Z. Q. Nie *et al.*, Phys. Rev. A **77**, 063829 (2008).
[18] M. D. Lukin, S. F. Yelin, M. Fleischhauer, and M. O. Scully, Phys. Rev. A **60**, 3225 (1999).
[19] M. Yan, E. G. Rickey, and Y. F. Zhu, Phys. Rev. A **64**, 013412 (2001).
[20] A. Joshi and M. Xiao, Phys. Lett. A **317**, 370 (2003).
[21] A. Joshi and M. Xiao, Phys. Rev. A **72**, 062319 (2005).
[22] A. Joshi and M. Xiao, Phys. Rev. A **71**, 041801 (2005).
[23] H. Y. Ling, Y. Q. Li, and M. Xiao, Phys. Rev. A **53**, 1014 (1996).
[24] B. Wang *et al.*, Opt. Lett. **31**, 3647 (2006).
[25] S. Li *et al.*, Phys. Rev. A **74**, 033821 (2006).
[26] B. Wang *et al.*, Phys. Rev. A **75**, 051801(R) (2007).
[27] Y. Han *et al.*, Phys. Rev. A **77**, 023824 (2008).
[28] S. Li *et al.*, Phys. Rev. Lett. **101**, 073602 (2008).
[29] M. Xiao, Y. Q. Li, S. Z. Jin, and J. Gea-Banacloche, Phys. Rev. Lett. **74**, 666 (1995).
[30] See document "Rubidium 85 D line data" in http://steck.us/alkalidata